Journal of Applied Physics

Observations regarding deep-level states causing p-type doping in AlTiO gate and positive threshold voltage shift in AlGaN/GaN high electron mobility transistors

Cite as: J. Appl. Phys. **130**, 015701 (2021); https://doi.org/10.1063/5.0053982
Submitted: 13 April 2021 • Accepted: 11 June 2021 • Published Online: 02 July 2021

Sayak Dutta Gupta, Vipin Joshi, Rajarshi Roy Chaudhuri, et al.

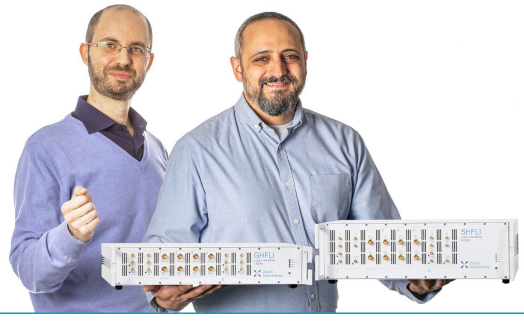

Journal of Applied Physics ARTICLE scitation.org/journal/jap

Observations regarding deep-level states causing p-type doping in AlTiO gate and positive threshold voltage shift in AlGaN/GaN high electron mobility transistors

Cite as: J. Appl. Phys. **130**, 015701 (2021); doi: 10.1063/5.0053982
Submitted: 13 April 2021 · Accepted: 11 June 2021 ·
Published Online: 2 July 2021

Sayak Dutta Gupta,[a] Vipin Joshi, Rajarshi Roy Chaudhuri, and Mayank Shrivastava[a]

AFFILIATIONS

Department of Electronic Systems Engineering, Indian Institute of Science, Bangalore 560012, India

[a]**Authors to whom correspondence should be addressed:** sayakgupta@iisc.ac.in and mayank@iisc.ac.in

ABSTRACT

Application of ternary oxides has emerged as a potential enabler to achieve enhancement mode (normally-OFF) operation in AlGaN/GaN high electron mobility transistors (HEMTs). However, it is not well understood what leads to the 2-Dimensional Electron Gas depletion or positive threshold voltage shift by the integration of these oxides in the gate stack. In this work, an electro-optical experiment-based method is used to probe the underlying mechanism. For experiments, AlGaN/GaN metal–oxide–semiconductor high electron mobility transistors with gate stack consisting of AlTiO (ternary p-type oxide), Al_2O_3, TiO_2 (undoped binary oxides), and NiO (conventional p-type oxide) are used. Optical exposure with wavelengths falling in the UV regime (365 nm) was found to induce a negative threshold voltage shift in AlTiO based devices. Experimentation on different GaN buffer stacks, different gate oxides, and selective UV exposure only to the gate region established the phenomenon to be governed by properties of the ternary oxide. This was further confirmed by the fact that the negative threshold voltage shift with UV exposure was proportional to the positive shift achieved as a function of Al% in AlTiO. The negative shift was found to be due to de-ionization of deep-level negative states in AlTiO, which resulted from the presence of Al at Ti sites ($[Al]'_{Ti}$). These negatively ionized deep-level states at room temperature result in p-type doping of the oxide, leading to the positive threshold voltage shift in AlTiO gate based HEMTs when compared with HEMTs with Al_2O_3 or TiO_2 as gate oxide.

I. INTRODUCTION

Design of gate dielectrics has emerged as a key enabler toward achieving high performance and reliable AlGaN/GaN power High Electron Mobility Transistors (HEMTs).[1–10] Inclusion of dielectric on top of the AlGaN barrier in the gate stack helps reduce gate leakage in the HEMTs besides allowing a larger gate overdrive. Development of Metal–Oxide–Semiconductor (MOS)-HEMTs is indeed essential for highly efficient and fail-safe normally-OFF operation, as the conventional Schottky-gated HEMTs have exceedingly high leakage during positive gate bias.

Ternary gate oxides, such as AlTiO, TiHfO, HfZrO, and HfAlO, have recently gained prominence as potential gate oxides for GaN MOSHEMTs.[2–7] The ternary systems have a unique ability to modulate oxide properties, such as dielectric constant (κ) and bandgap (E_g) among others, to achieve desirable oxide properties. In our recent work, Al% in ternary oxide $Al_xTi_{1-x}O_y$ was demonstrated to be a tuning parameter to control p-type property of AlTiO.[4] This enabled us to demonstrate normally-OFF MOSHEMTs with performance at par with state of the art HEMTs.[4] These unique features offered by AlTiO resulted in an increased interest in the community for optimizing and characterizing this ternary oxide.[3–5] However, a comprehensive understanding of the nature of Al alloying in AlTiO, which helps in achieving the unique HEMT performance, is still elusive. The wide E_g nature of III–nitrides, ternary oxide, and multiple interfaces in AlGaN/GaN MOSHEMTs makes the characterization of deep states in such oxides and probing the root cause a challenging task.[11,12] Moreover, while well-established high-κ (HfO_2, ZrO_2) and conventional (Al_2O_3, SiN_x, SiO_2) dielectric based GaN MOSHEMTs still

suffer from reliability challenges,[13–18] very few reports are available on the robustness of ternary gate oxide-based GaN devices.

Keeping these issues in mind and limited work available on the physical understanding and reliability of ternary gate oxides for AlGaN/GaN MOSHEMTs, this work demonstrates an electro-optical experiment-based method to probe the physical mechanism governing positive threshold voltage (V_{th}) shift in AlTiO-based GaN HEMTs with different Al%. Experimentation of MOSHEMTs and MOS Capacitors (MOSCAPs) with different gate oxides and different buffer stacks is carried out to establish that the phenomenon is governed by deep-level negative states due to Al at Ti sites, which also controls the p-type doping concentration in the oxide. The paper is organized as follows. The device fabrication and experimental setup are discussed in Sec. II. The physical mechanism governing the positive V_{th} shift in AlTiO-based GaN devices is studied in Sec. III. The proposed mechanism is validated in Sec. IV by varying the exposure time and probing the recovery behavior. Finally, this work is concluded in Sec. V.

II. DEVICE FABRICATION AND EXPERIMENTATION

MOCVD grown C-doped GaN on Si epi-stack with 3 nm GaN capping layer (stack 1) was used for this work. The grown epi-stack (stack 1) had a 2-DEG density of $\sim 8 \times 10^{12}\,\mathrm{cm}^{-2}$. AlGaN/GaN MOSHEMTs and MOSCAPs, as seen in Figs. 1(a) and 1(b), were then processed on stack 1 using a well-optimized process flow.[4] Moreover, in order to have a GaN buffer variant, devices were also fabricated on an epi-stack consisting of thicker C-doped GaN buffer with different C-doping (stack 2). The fabrication started with partially recessing the AlGaN barrier followed by deposition of Ti/Al/Ni/Au and 820 °C 30 s N_2 anneal for source/drain ohmic contact formation. The devices were then isolated using Cl_2/BCl_3 plasma etching. Gate oxides were then deposited following a dilute HCl based surface cleaning. Finally, a 20/70 nm film of Ni/Au was deposited as gate metal followed by a 300 °C 10 min anneal in forming gas ambient to form the GaN MOSHEMTs and MOSCAPs, as seen in Figs. 1(c) and 1(d), respectively. It is worth highlighting here that the thin gate metal was chosen to allow penetration of 365 nm UV.

Amorphous gate oxides were deposited using a BENEQ thermal atomic layer deposition (ALD) system. While Al_2O_3 was deposited in the ALD system at 250 °C using trimethylaluminum (TMA) and water, TiO_2 was grown using titanium tetraisopropoxide (TTIP) and water at 200 °C. Furthermore, sequential deposition of Al_2O_3 and TiO_2 at 250 °C in ALD was used to develop $Al_xTi_{1-x}O_y$, with the ratio of Al_2O_3 and TiO_2 cycles controlling the Al% in AlTiO, which is reported in detail in Ref. 4. The following ALD oxides were deposited: (a) undoped binary oxide: 14 nm Al_2O_3 ($\kappa \sim 9$, $E_g \sim 7\,\mathrm{eV}$[3]) and 10 nm TiO_2 ($\kappa \sim 75$, $E_g \sim 3.4 - 3.7\,\mathrm{eV}$[19]) and (b) p-type ternary oxide $Al_xTi_{1-x}O_y$

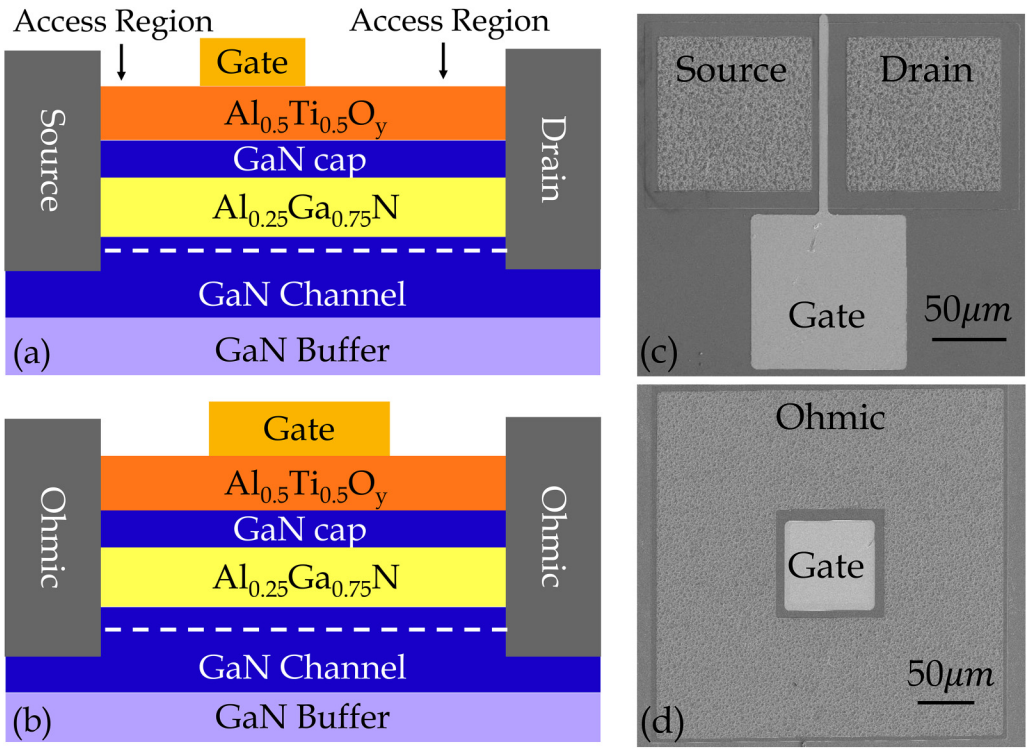

FIG. 1. Cross-sectional view of the AlGaN/GaN (a) MOSHEMT and (b) MOS Capacitors with p-type metal oxide ($Al_{0.5}Ti_{0.5}O_y$) gate. Similar devices were also processed with different gate dielectrics. FESEM images of the processed AlGaN/GaN (c) MOSHEMT and (d) MOS Capacitor.

(AlTiO) with varied x. The AlTiO oxides deposited are 7 nm $Al_{0.1}Ti_{0.9}O_y$ ($\kappa \sim 50$), 10 nm $Al_{0.2}Ti_{0.8}O_y$ ($\kappa \sim 35$), and 14 nm $Al_{0.5}Ti_{0.5}O_y$ ($\kappa \sim 25$). While increasing Al% in AlTiO does reduce κ, E_g of AlTiO almost linearly increases from the E_g of TiO_2 to Al_2O_3 with an increase in Al% (E_g of $Al_{0.5}Ti_{0.5}O_y$ $\sim 5.5\,eV$).[3] Moreover, the introduction of Al in TiO_2 also results in a p-type doping,[4] with $Al_{0.5}Ti_{0.5}O_y$ exhibiting a majority hole concentration of $1.4 \times 10^{14}\,cm^{-3}$ at room temperature, as measured using Hall setup. It is worth highlighting here that despite having low E_g, TiO_2, and AlTiO with lower Al% are also used in this work, to gain physical insight into the role of Al% in determining V_{th} shift in AlTiO based AlGaN/GaN HEMTs. Furthermore, besides the ALD oxides, conventional binary p-type oxide NiO was also deposited as gate oxide using e-beam evaporation.

Figure 2(a) shows the GaN MOSHEMTs with Al_2O_3 and TiO_2 gate to have a significantly negative V_{th}, indicating depletion mode operation. The negative V_{th} in Al_2O_3 and TiO_2 gated GaN HEMTs is attributed to positively charged Al_2O_3/GaN and TiO_2/GaN interface[20,21] with an interface charge density of the order of $\sim 10^{12} - 10^{13}\,cm^{-2}$.[22] Moreover, the use of 14 nm of low-κ Al_2O_3 as compared to 10 nm of high-κ TiO_2 also resulted in a weaker gate control and more negative V_{th} in the Al_2O_3-gated GaN MOSHEMTs. Introduction of Al in TiO_2, however, resulted in a positive shift in V_{th} in the HEMTs. The Al% in AlTiO controls the p-type doping concentration in the gate oxide and thereby determines the positive V_{th} shift, as was reported in our earlier work.[4] The HEMTs under test show a comparable ON-state and OFF-state performance, irrespective of the gate stack, as seen in Figs. 2(a) and 2(b).

Current–voltage (I–V) characterizations of the devices were carried out in dark (pre-UV exposure) and post-365 nm UV exposure (post-UV exposure). On the other hand, capacitance–voltage (C–V) device characterizations were carried out in dark (pre-UV exposure) and under 365 nm UV exposure (under UV exposure) to prevent any recovery during the longer C–V measurements. A 365 nm non-coherent UV source was used for optical exposure to reduce electron–hole pair generation in the AlGaN/GaN system.[23]

III. PROBING THE PHYSICAL MECHANISM

A. Possible source responsible for positive V_{th} shift

AlTiO has recently been demonstrated as a p-type gate oxide for AlGaN/GaN MOSHEMTs,[4] where Al% controls the p-type doping concentration and hence the device V_{th}, as seen in Fig. 2(a). The process governing the introduction of p-type nature by incorporation of Al in TiO_2 can be explained from the Kröger–Vink notation based defect reaction for introduction of Al_2O_3 in TiO_2, as seen in Eqs. (1) and (2),[4]

$$Al_2O_3 \overset{2TiO_2}{\Longleftrightarrow} 2[Al]'_{Ti} + 3[O]_O + [V]^{\bullet\bullet}_O, \tag{1}$$

$$[V]^{\bullet\bullet}_O \Longleftrightarrow [V]_O + 2h^{\bullet}. \tag{2}$$

Equation (1) shows creation of negatively charged Al fixed charges occupying Ti sites ($[Al]'_{Ti}$) and positively charged oxygen vacancy ($[V]^{\bullet\bullet}_O$) by introduction of Al_2O_3 in TiO_2. $[V]^{\bullet\bullet}_O$ results in a neutral oxygen vacancy ($[V]_O$) and introduces holes ($h^{\bullet}$) in the system, as seen in Eq. (2). This results in p-type doping of Al alloyed TiO_2. The negative states in the gate stack will deplete the 2-DEG under the gate as depicted in Fig. 3. The channel depletion in turn results in a positive shift in V_{th}. Moreover, increasing Al% in AlTiO would increase the concentration of the negatively charged states $[Al]'_{Ti}$, which in turn will increase the p-type doping concentration of the oxide, causing an additional positive shift in V_{th}, as seen in Fig. 2(a).

These negative states, which result in the p-type doping of AlTiO, should behave as traps. Trap characterization techniques can hence be employed to gain insights into the physical mechanism of these ternary systems. However, wider bandgap of AlTiO combined with multiple interfaces in GaN HEMTs poses challenges in probing traps in such oxides. Sections III B–III F deal with probing these oxide traps using a electro-optical technique proposed in this work.

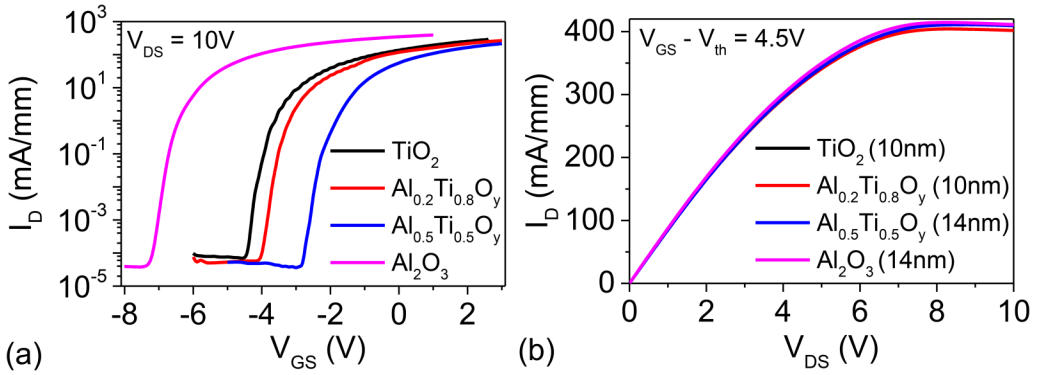

FIG. 2. (a) Transfer (I_D–V_{GS}) characteristics and (b) output (I_D–V_{DS}) characteristics of the fabricated AlGaN/GaN MOSHEMTs. The HEMTs showed similar ON- and OFF-state performance, irrespective of the gate stack. The threshold voltage (V_{th}) of the $Al_{0.5}Ti_{0.5}O_y$-gated HEMTs was significantly positively shifted due to the p-type property of the oxide.

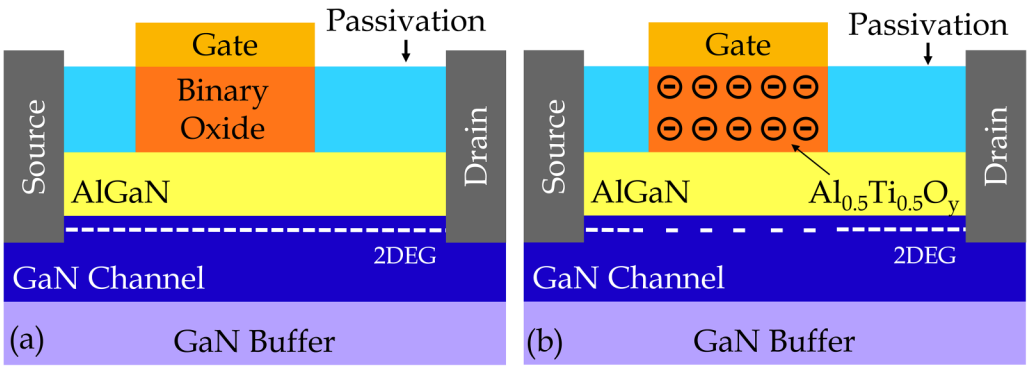

FIG. 3. Schematic of AlGaN/GaN MOSHEMTs with (a) undoped binary oxides, such as Al_2O_3 and TiO_2, and (b) p-type ternary oxide $Al_{0.5}Ti_{0.5}O_y$, as gate oxides. The AlTiO-based GaN devices show a reduced 2-DEG density under the gate due to negatively ionized states, which induce the p-type doping in AlTiO.

B. Characterizing traps in wide E_g gate oxides

Figure 4(a) shows the dual sweep transfer (I_D–V_{GS}) characteristics of the fabricated $Al_{0.5}Ti_{0.5}O_y$-gated MOSHEMTs for V_{DS} of 1 and 10 V. The HEMTs showed negligible hysteresis, irrespective of the V_{DS}, which indicates the superior oxide/III-nitride interface of the devices. In order to further analyze the interface quality, hysteresis and frequency dispersion in the C–V curve were studied, which are well-established techniques to determine interface quality.[2,8,24–26] Figure 4(b) shows the dual sweep C–V curve of the $Al_{0.5}Ti_{0.5}O_y$ based AlGaN/GaN MOSCAPs over a frequency range of 10 KHz–1 MHz. The devices showed typical two-step C–V characteristics with the first step signifying the transition from depletion to accumulation of 2-DEG at the AlGaN/GaN interface. The injection of electrons from AlGaN/GaN to oxide/nitride interface is then reflected as the second step of the C–V curve. The MOSCAPs showed negligible hysteresis in both the steps irrespective of the measurement frequency, as seen in Fig. 4(b). This further establishes the superior quality of the AlTiO/nitride interface. However, the second step of the $Al_{0.5}Ti_{0.5}O_y$ based GaN MOSCAPs showed significant frequency dispersion, as seen in Fig. 4(b). This is generally an effect of high interface trap density.[26] The conductance method is one of the standard methods to evaluate these interface traps.[2,5,27] However, it has a limited capability of probing only shallow traps in this wide E_g oxide.[5] Moreover, Capriotti *et al.*[28] have established the method to be incapable of evaluating interface traps in AlGaN/GaN MOS devices due to the presence of AlGaN barrier.

It is, therefore, important to investigate traps in these novel and wide E_g ternary systems using unique characterization approaches. The necessary condition for probing deep traps is to excite them, which can be achieved by high energy photons. Hence, an electro-optical based technique is used in this work to characterize the AlTiO/GaN system, which is discussed in Secs. III C–III F.

C. Impact of UV photon exposure—negative V_{th} shift

In order to probe into energetically deeper traps in the developed ternary oxide, devices were subjected to high energy photon (365 nm, UV) exposure. $I_D - V_{GS}$ curves measured before exposing

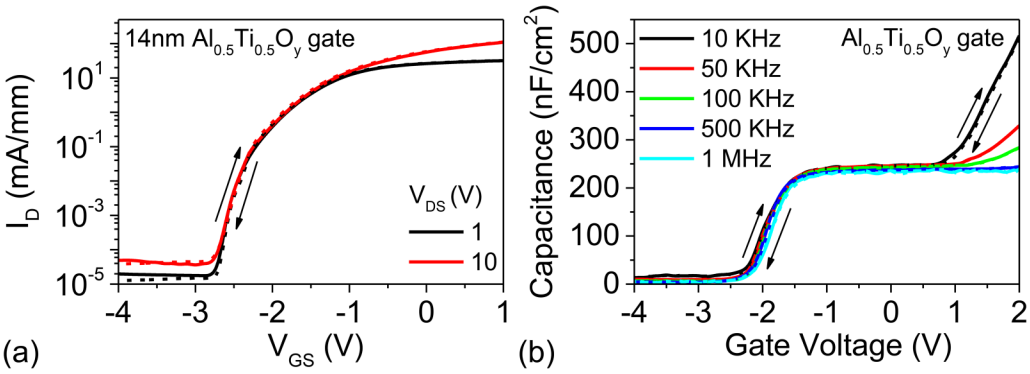

FIG. 4. (a) Dual sweep I_D–V_{GS} characteristics of the $Al_{0.5}Ti_{0.5}O_y$-gated HEMTs showing negligible hysteresis irrespective of V_{DS}. (b) Dual sweep C–V characteristics of the $Al_{0.5}Ti_{0.5}O_y$-based MOSCAPs, as a function of frequency, also show negligible hysteresis. The MOSCAPs, however, showed a high frequency dispersion.

the device to UV photons and after exposing the device (in unbiased condition) to UV photons for 60 s are compared in Fig. 5(a). Measurements done before and after the UV exposure are referred to as pre-UV exposure and post-UV exposure measurements, respectively. It reveals a negative shift in V_{th} (ΔV_{th}) and an increase in OFF-state leakage due to the UV exposure. Here, $\Delta V_{th} = V_{th,\,Post\ UV} - V_{th,\,Pre\ UV}$, where $V_{th,\,Pre\ UV}$ is the device's pristine V_{th} and $V_{th,\,Post\ UV}$ is the V_{th} induced by 365 nm UV exposure. Moreover, an UV exposure time of 60 s was found to induce maximum V_{th} shift in the device and, hence, was used for analysis here. The time dependence of UV induced V_{th} shift will be discussed in Sec. IV A. Figure 5(a) also reveals the observed ΔV_{th} to be a strong function of the gate oxide. While the Al_2O_3- and TiO_2-gated GaN MOSHEMTs showed a minor shift of ~ -0.3 V, the $Al_{0.5}Ti_{0.5}O_y$ based HEMTs showed a distinctive ΔV_{th} of -1.5 V, as seen in Fig. 5(a). This large ΔV_{th} in $Al_{0.5}Ti_{0.5}O_y$ gated devices after exposure to UV light suggests the presence of deep-level traps being excited by UV exposure. It is worth highlighting here that the $I_D - V_{GS}$ sweeps for Al_2O_3- and $Al_{0.5}Ti_{0.5}O_y$-gated MOSHEMTs were measured immediately after the UV exposure to minimize time-dependent recovery of the devices. However, such an attempt in the TiO_2-gated HEMTs resulted in device failure, which is attributed to smaller E_g of TiO_2 resulting in a significant increase in gate leakage due to UV exposure. The TiO_2-gated HEMTs had to be given a $\sim$60 s relaxation after UV exposure to conduct $I_D - V_{GS}$ measurements without failing the device.

It was observed that performing C–V measurements on the devices even under the UV exposure did not result in device failure. Therefore, in order to do a comparative analysis of ΔV_{th} for devices with different gate oxides under similar bias conditions, C–V analysis was carried out under UV exposure. Moreover, devices were first subjected to a 60 s UV exposure before beginning the C–V measurements to ensure maximum V_{th} shift. The C–V characteristics of GaN MOSCAPs with different gate oxides are shown in Fig. 5(b). Negative V_{th} shifts, similar to that observed in the MOSHEMTs in Fig. 5(a), were also seen for the MOSCAPs. This definitive ΔV_{th} of -1.5 V in the $Al_{0.5}Ti_{0.5}O_y$-based GaN MOSCAPs under UV exposure, unlike the MOSCAPs with other gate oxides, clearly signifies the presence and excitation of deep-level oxide traps in $Al_{0.5}Ti_{0.5}O_y$ using UV. Furthermore, the absence of such a V_{th} shift in the binary gate oxides suggests the observed phenomenon to be related to Al introduced in TiO_2.

D. Role of Al% in AlTiO on the V_{th} shift

Section III C demonstrated a UV exposure induced V_{th} shift unique to ternary oxide AlTiO. In order to further evaluate role of Al% in determining V_{th} shift observed in AlTiO based GaN devices, ΔV_{th} of $Al_xTi_{1-x}O_y$-based GaN MOSCAPs with varied Al % was studied, as seen in Fig. 6(a). Figure 6(a) shows ΔV_{th} in these devices to significantly increase with increasing Al% in AlTiO. It is worth highlighting here that increasing Al% also increases the p-type doping concentration in the oxide, thereby increasing the V_{th},[4] as seen in Fig. 2(a). Binary p-type oxides, such as NiO, based GaN MOSCAPs, however, show a much lower ΔV_{th} of -0.8 V, as seen in Fig. 6(b). These observations point toward deep-level traps in the ternary p-type AlTiO to be responsible for the significant negative V_{th} shift in these devices under UV exposure. However, hetero-epitaxially grown AlGaN/GaN on Si is known to have traps in multiple locations, thereby necessitating detailed analysis to ascertain the location of the deep traps that are responsible for this V_{th} shift under 365 nm UV exposure.

E. What may cause the V_{th} shift?

The above discussion establishes the observed phenomena to be related to AlTiO. In order to further rule out the possibility of UV assisted trapping/de-trapping in the GaN buffer region to cause the observed V_{th} shift, p-type $Al_{0.5}Ti_{0.5}O_y$-gated devices were also processed on a high breakdown voltage commercial-grade C-doped GaN on Si stack (stack 2). Figure 7(a) compares the photoluminescence (PL) spectra of the two GaN buffer stacks, stack 1 and stack 2, measured using a 325nm laser. The yellow (YL) and blue luminescence (BL) bands in the spectra indicate the presence of C-doping in both the GaN buffers.[29] Moreover, stack 1 has a relatively higher

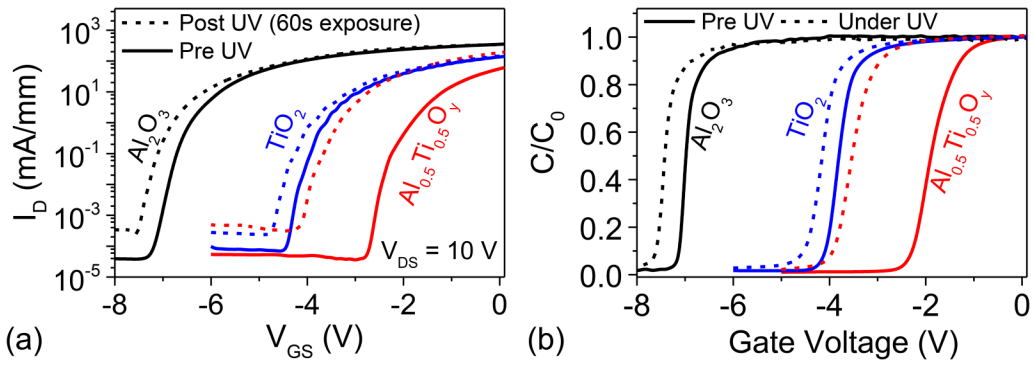

FIG. 5. (a) I_D–V_{GS} characteristics of MOSHEMTs with different gate stacks measured pre-and post-60 s 365 nm UV exposure. (b) C–V characteristics of MOSCAPs with different gate stacks measured pre- and under 365 nm UV exposure. Here, the $I_D - V_{GS}$ measurements were carried out on GaN MOSHEMTs immediately after UV exposure, whereas C–V measurements were done on MOSCAPs under 365 nm UV exposure. While the Al_2O_3- and TiO_2-gated GaN devices showed a ~ -0.3 V shift in V_{th} due to UV exposure, a -1.5 V shift was observed in the $Al_{0.5}Ti_{0.5}O_y$-gated GaN MOS devices. Besides, C_0 is the accumulation capacitance of the MOSCAPs.

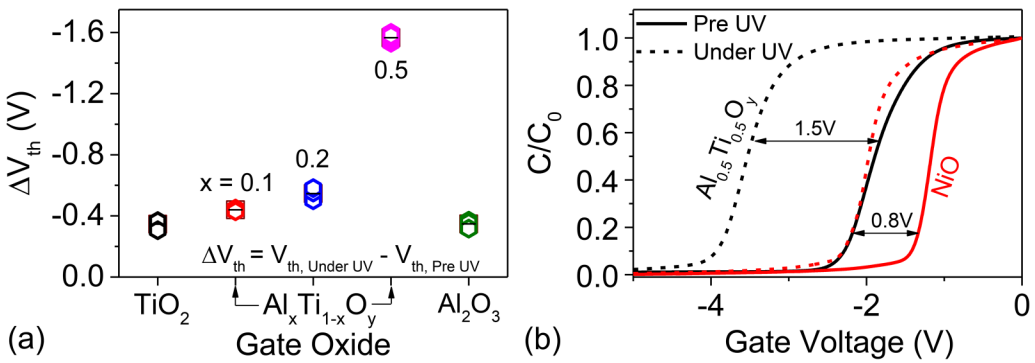

FIG. 6. (a) UV induced V_{th} shift, measured as $\Delta V_{th} = V_{th,\ Under\ UV} - V_{th,\ Pre\ UV}$, for different gate oxides in GaN MOSCAPs. TiO_2- and Al_2O_3-based AlGaN/GaN MOSCAPs showed a mere −0.3 V shift under UV exposure. However, introduction of Al in TiO_2 ($Al_xTi_{1-x}O_y$-based gate oxides) significantly increased the ΔV_{th} in the devices with Al% controlling the shift. (b) Normalized capacitance (C/C_0) of p-type gate oxide-based AlGaN/GaN MOSCAPs pre- and under 365 nm UV photon exposure. Here, C_0 is the accumulation capacitance of the MOSCAPs.

C-doping than stack 2, which is confirmed from the higher BL in the PL spectra of stack 1.[29] Figure 7(b) compares the C–V characteristics of $Al_{0.5}Ti_{0.5}O_y$-based GaN MOSCAPs fabricated on these stacks, in pristine (pre-UV exposure) and under 365 nm UV exposure conditions. A thinner barrier layer under the gate results in the MOSCAPs on Stack 2 to have a ∼1 V positive V_{th} pre-UV exposure as compared to Stack 1. However, the MOSCAPs showed a similar ΔV_{th} of ∼−1.5 V irrespective of the GaN buffer stack. This further establishes deep traps present in $Al_{0.5}Ti_{0.5}O_y$ to be the source of V_{th} shift in these devices and the observed shift to be independent of GaN buffer properties.

However, considering blanket deposition, AlTiO is present in gate as well as access region, as shown in Fig. 1(a). In order to further probe into the effect based on the location of AlTiO, GaN MOSCAPs were subjected to selective 365 nm UV exposure only over the gate area (selective gate exposure). A comparison of ΔV_{th} for devices subjected to selective gate exposure with devices subjected to complete device (flood) exposure, as shown in Fig. 7(c), reveals a similar ΔV_{th} in both the cases. Moreover, the observed ΔV_{th} was found to be independent of gate area, as shown in Fig. 7(c). These observations establish that the 365 nm UV penetrates the thin gate metal and the observed ΔV_{th} is due to trap excitation in the $Al_{0.5}Ti_{0.5}O_y$ beneath the gate.

F. The phenomena governing V_{th} modulation in ternary oxides

As discussed above, 365 nm UV exposure induced a significantly higher negative V_{th} shift in AlTiO based AlGaN/GaN devices with the shift being strongly related to Al% in the oxide. Furthermore, Al induced deep-level traps in AlTiO gate oxide were established to be the source of this shift. This is in agreement with the proposal on the source of positive V_{th} shift in AlTiO-gated HEMTs in Sec. III A and can be explained as follows.

The ternary oxide AlTiO, formed by introduction of Al_2O_3 in TiO_2, results in creation of negatively charged Al fixed charges occupying Ti sites ($[Al]'_{Ti}$), neutral oxygen vacancies ($[V]_O$) and holes ($h^\bullet$), as seen in Eqs. (1) and (2). These negative states deplete

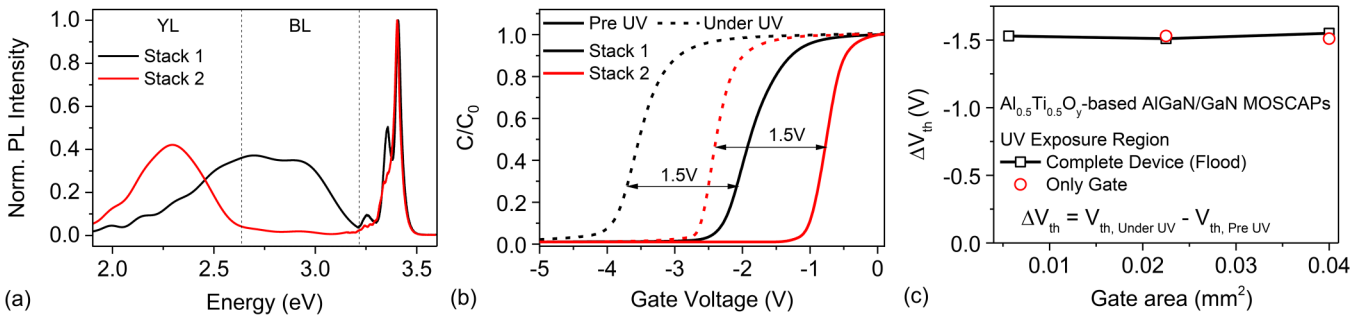

FIG. 7. (a) Photoluminescence (PL) spectra of the GaN buffer stacks used for this work obtained using a 325 nm laser. Yellow (YL) and blue luminescence (BL) bands in the spectra show both the stacks to be C-doped, with stack 1 having a higher C-doping as compared to stack 2. (b) Normalized capacitance (C/C_0) of the $Al_{0.5}Ti_{0.5}O_y$-based AlGaN/GaN MOSCAPs show a V_{th} shift of −1.5 V under 365 nm UV exposure, irrespective of the GaN buffer. Here, C_0 is the accumulation capacitance of the MOSCAPs. (c) Shift in V_{th} with varied UV exposure region, measured as $\Delta V_{th} = V_{th,\ Under\ UV} - V_{th,\ Pre\ UV}$, as a function of gate area.

the 2-DEG under the gate (n_s), as seen in Fig. 8(a). This is further experimentally observed from C–V sweeps on MOSCAPs shown in Fig. 8(d). Figure 8(d) shows that n_s under the gate shows a significant dependence on Al% in AlTiO gate oxide. $Al_{0.5}Ti_{0.5}O_y$-based GaN devices have a significantly lower n_s under gate in pristine condition and thereby a positively shifted V_{th}.

The negative states induced by Al de-ionize upon UV exposure, as depicted in Figs. 8(b) and 8(c). This results in an increase in 2-DEG density underneath the gate electrode. This is further experimentally seen in Fig. 8(d), which shows similar 2-DEG density in the devices under UV exposure, irrespective of the gate oxide. AlTiO gate oxides with higher Al% have a higher concentration of deep-level negative states $[Al]'_{Ti}$, thereby resulting in a higher V_{th} shift under UV exposure. Above discussion establishes that concentration of $[Al]'_{Ti}$ determines the extent of positive V_{th} shift (p-type doping concentration) in the AlTiO-gated GaN devices.

Besides, E_g of AlTiO is known to increase with Al%.[3] The p-type nature exhibited by $Al_xTi_{1-x}O_y$ in room temperature[4] irrespective of its wide E_g (which increases with 'x') suggests that the $[Al]'_{Ti}$ acceptor states (E_T) in the oxide bulk are close enough to the valence band (E_V) to be ionized at room temperature. Given the wide E_g (~5.5 eV for x = 0.5) of the oxide,[3] it is difficult to de-trap the electrons from these states ($[Al]'_{Ti}$) to the oxide conduction band (E_C) under 365 nm UV exposure (~3.4 eV). However, the $[Al]'_{Ti}$ traps at and in close proximity to the oxide/III–N interface (~ few nm) can respond to the UV excitation by being injected into the III–N layer (GaN cap or AlGaN barrier), as seen in Fig. 8(c). The energy barrier for such injection is lowered (as compared to the trap-level oxide conduction band excitation) by two factors: (1) conduction band offset at the oxide/III–nitride hetero-junction and (2) strong polarization field induced band bending in the III–N layer. The de-trapped electrons injected into the III–N layer can be swept toward the AlGaN/GaN quantum well, subsequently increasing the 2-DEG density, as shown in Fig. 8(c).

Above observations and discussion establish the presence of negatively ionized deep-level states ($[Al]'_{Ti}$) at and near the oxide/nitride interface under the gate metal with Al% in $Al_xTi_{1-x}O_y$ controlling the concentration of these states. The presence of these negative states at/near the interface results in p-type nature of the oxide and significant positive V_{th} shift in AlTiO based devices, besides requiring an electro-optical approach to examine the p-type property. This study thereby helps attain a deeper insight into the physical mechanism governing the positive V_{th} shift in AlTiO-gated AlGaN/GaN MOSHEMTs, as reported in Ref. 4 and seen in Fig. 2.

IV. VALIDATION: TIME RESPONSE AND V_{th} RECOVERY

A. V_{th} shift as a function of exposure time

While the discussion till now was based on a fixed UV exposure time, Fig. 9 depicts the exposure time dependence of ΔV_{th} in $Al_{0.5}Ti_{0.5}O_y$-based GaN MOSHEMTs. This is studied to ensure that the UV exposure does not introduce any defect state. Figure 9(a) shows significant dependence of ΔV_{th} and OFF-state leakage in the HEMTs on UV exposure time, however only till 60 s of exposure. The ΔV_{th} is seen to increase from ~ −0.4 V for 5 s UV exposure to as high as −1.5 V for exposure time of 60 s, as seen in Fig. 9(b). Any further increase in the UV exposure time has a negligible impact on V_{th} shift or leakage. The saturation in ΔV_{th} and OFF-state drain leakage for longer exposure times is further validated in Fig. 10. Figures 10(a) and 10(b) monitor the drain (I_D) and gate (I_G) currents of the $Al_{0.5}Ti_{0.5}O_y$-gated MOSHEMTs over time for multiple UV exposures with the device being biased in ON-state and OFF-state, respectively. The UV exposure resulted in ~2 orders increase in I_G, irrespective of the bias state. However, while the UV induced I_D increase was due to I_G in OFF-state, the same in ON-state was due to negative V_{th} shift. Furthermore, the change in I_D (V_{th}) and I_G is seen to saturate for longer UV exposures, as was also observed in Fig. 9. Figures 9 and 10 show that UV excites only the existing deep-level traps in the system, and no new trap states were created. The long UV exposure required for significant V_{th} shift and the saturation in I_D (V_{th}) and I_G for longer UV exposures also establish AlTiO as a reliable ternary oxide for

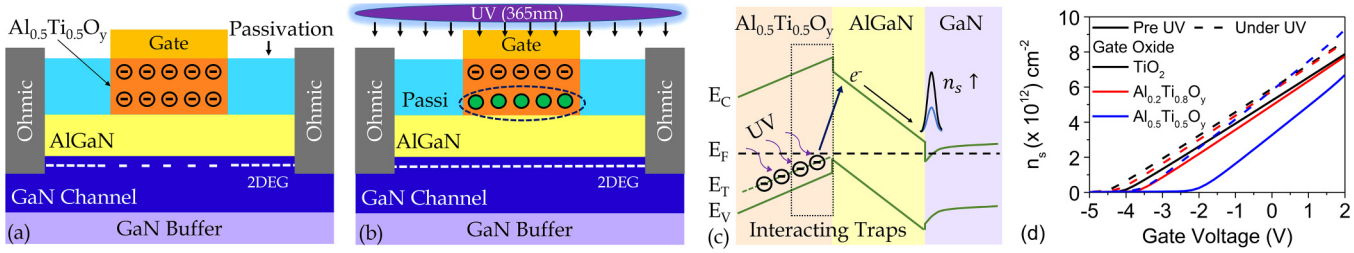

FIG. 8. Schematic of $Al_{0.5}Ti_{0.5}O_y$-based AlGaN/GaN devices depicting (a) reduced 2-DEG density under the gate due to Al induced negatively ionized states ($[Al]'_{Ti}$) in p-type AlTiO and (b) increase in 2-DEG density under the gate due to UV induced de-ionization of the negatively charged states inside AlTiO. (c) Schematic band diagram of $Al_{0.5}Ti_{0.5}O_y$-based AlGaN/GaN devices depicting excitation of the negatively charged ($[Al]'_{Ti}$) deep-level traps at and near the AlTiO/III–N interface only, by 365 nm UV, to result in an increase in 2-DEG density, as $Al_{0.5}Ti_{0.5}O_y$ has a significantly higher bandgap than the photon energy. This $[Al]'_{Ti}$ trap concentration would determine the 2-DEG density under the gate, thereby determining the shift in V_{th} in these devices. (d) Experimentally obtained channel 2-DEG density (n_s) in AlGaN/GaN MOSHEMTs with various gate oxides pre- and under 365 nm UV exposure. The n_s obtained from C–V sweeps on MOSCAPs with 200 × 200 μm^2 gate pads and gate-ohmic pad spacing of 5 μm helps to measure 2-DEG under the gate effectively. Increase in Al% in AlTiO is seen to reduce the pristine 2-DEG density under the gate, thereby resulting in a positive shift in V_{th}. Similar n_s, irrespective of gate oxides, is, however, observed under 365 nm UV photon exposure.

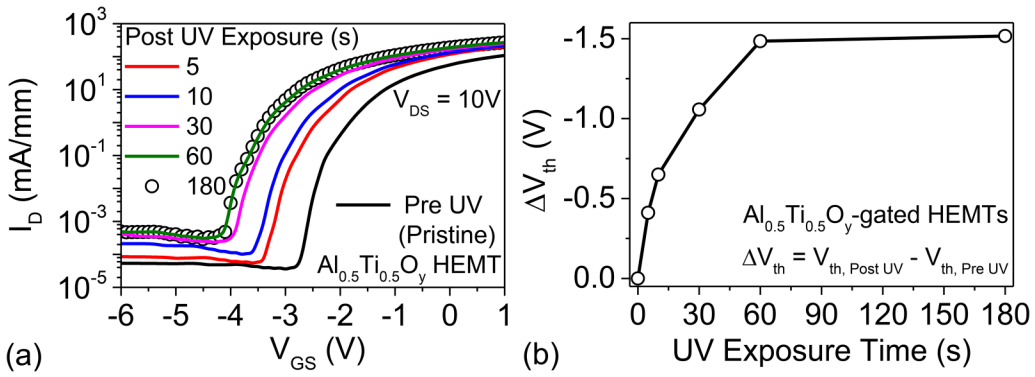

FIG. 9. (a) I_D–V_{GS} characteristics of the $Al_{0.5}Ti_{0.5}O_y$-gated MOSHEMTs measured immediately post-UV exposure as a function of exposure time. (b) The V_{th} shift, measured as $\Delta V_{th} = V_{th,\ Post\ UV} - V_{th,\ Pre\ UV}$. Here, $V_{th,\ Pre\ UV}$ and $V_{th,\ Post\ UV}$ are threshold voltages measured before and after UV photon exposure, respectively.

GaN MOSHEMTs. This is further verified from Fig. 10, which shows the devices to start recovering post-UV exposure.

B. Post-UV V_{th} recovery

The time based recovery of the devices post-UV photon exposure, as seen in Fig. 10, reveals a slower I_D recovery for devices biased at V_{GS} of −1 V [Fig. 10(a)] as compared to recovery for devices biased at a V_{GS} of −6 V [Fig. 10(b)]. This necessitates evaluating the impact of relaxation time and negative gate bias on the V_{th} recovery. C–V sweeps of $Al_{0.5}Ti_{0.5}O_y$-based GaN MOSCAPs, as seen in Fig. 11(a), show an incomplete V_{th} recovery even post a 600 s relaxation period. Furthermore, to evaluate the impact of V_{GS} on device recovery, the ratio of measured capacitance to pristine capacitance of the devices at $V_G = -2V$ $(C/C_{pristine}@-2V)$ during UV photon exposure and post-exposure is studied, as depicted in Fig. 11(b). The $C/C_{pristine}@-2V$ is seen to increase by ∼3× under UV exposure, which starts reducing with repeated C–V sweeps post the exposure. However, this recovery is seen to be a strong function of the sweep voltage. While a dual C–V sweep from 0 to −2 V does not completely recover the $C@-2V$ despite four repeated sweeps ($C/C_{pristine}@-2\,\mathrm{V} = 2$), a 0 to −5 V dual C–V sweep ensures complete recovery after two sweeps. The observed faster V_{th} recovery for higher negative V_{GS} can be explained as follows: device recovery requires ionization of the deep-level traps (Al fixed charges) $[Al]_{Ti}$, which can be achieved by electron injection into the oxide. As negative gate bias would increase electron injection across the gate oxide, negative gate bias dependent recovery is seen in these devices.

The above discussion establishes that the higher (positive) threshold voltage observed in HEMTs with AlTiO gate oxide is due to deep-level states, which result in p-type doping in AlTiO. These deep-level negative states in AlTiO, however, remain stable under regular stress conditions, as seen from dual sweep I–V and C–V in Fig. 4, and require high energy UV photons for the de-ionization. It can also be concluded that the proposed approach to probe deep-level states does not adversely affect the performance and reliability behavior of AlTiO gate HEMTs. These observations also establish AlTiO to be a stable and reliable p-type ternary gate oxide for AlGaN/GaN MOSHEMTs.

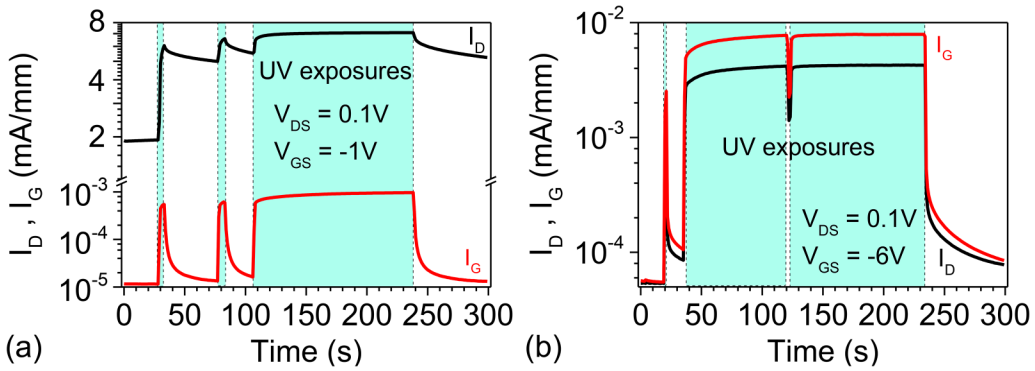

FIG. 10. Drain (I_D) and gate (I_G) currents of the $Al_{0.5}Ti_{0.5}O_y$-gated MOSHEMTs monitored during the UV photon exposure as well as post-UV exposures in (a) ON-state and (b) OFF-state.

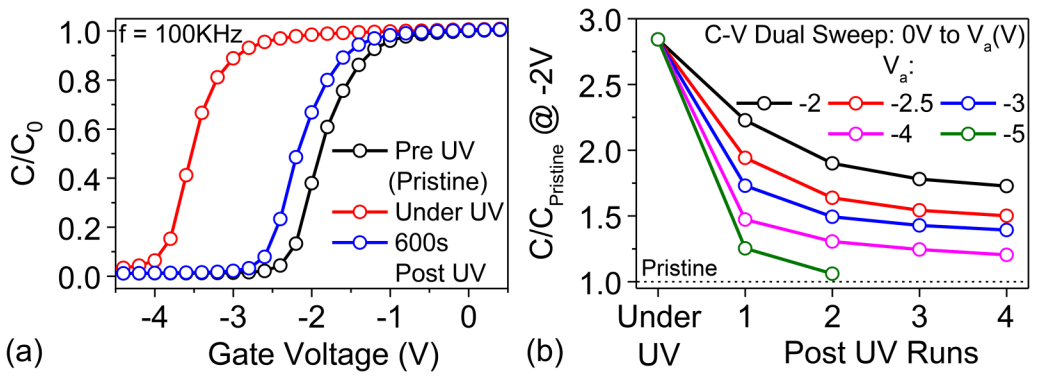

FIG. 11. (a) Normalized capacitance (C/C_0) of the $Al_{0.5}Ti_{0.5}O_y$-based AlGaN/GaN MOSCAPs extracted under different exposure conditions. Here, C_0 is the accumulation capacitance of the MOSCAPs. (b) The capacitance of the MOSCAPs, under and post-365 nm UV photon exposure, at −2 V normalized to its pristine value ($C/C_{pristine}@-2$ V).

V. CONCLUSION

AlGaN/GaN MOSHEMTs with ternary AlTiO as gate oxide exhibit a significantly higher (positive) threshold voltage when compared to threshold voltage often measured in HEMTs with binary oxides. This makes gate stacks with AlTiO a potential enabler or alternative for enhancement mode operation in HEMTs. In this work, we demonstrated an electro-optical method to gain insights into the physical mechanism governing this positive threshold voltage shift in GaN HEMTs having AlTiO (Al alloying in TiO_2) as gate oxide. A significant negative shift in threshold voltage of HEMTs with AlTiO as gate oxide was observed when measurements were conducted together with UV photon exposure. However, this shift was found to be independent of buffer doping and gate area. Furthermore, threshold voltage shift under similar conditions was found to be negligible in HEMTs having undoped binary gate oxides, such as Al_2O_3, TiO_2 (~ -0.3 V), and marginal in p-type NiO (~ -0.8 V), confirming that the observed behavior is unique to p-type ternary oxides like AlTiO. This was further confirmed by the fact that the negative threshold voltage shift with UV exposure was proportional to the positive shift achieved as a function of Al% in AlTiO. This shift in AlTiO gated HEMTs during UV exposure was found to be due to de-ionization of deep-level negative states in AlTiO, which resulted from the presence of Al at Ti sites ($[Al]'_{Ti}$). These negatively ionized deep-level states at room temperature were found to be predominantly present at/near the oxide/nitride interface under the gate metal. Moreover, these ionized states result in p-type doping of the oxide, leading to the positive threshold voltage shift in AlTiO gate based HEMTs when compared with HEMTs employing Al_2O_3 or TiO_2 as gate oxide. Negative threshold voltage shift post-UV exposure was found to recover with time. The recovery can be accelerated with the application of negative gate voltage. It was also shown that the proposed approach to probe deep-level states does not adversely affect the performance and reliability behavior of AlTiO-gated HEMTs. A high exposure time (~60 s) required for the threshold voltage shift, fixed shift, and observed recovery phenomena post-UV exposure establish AlTiO as a reliable gate oxide for AlGaN/GaN HEMTs.

ACKNOWLEDGMENTS

This work was supported by the Department of Science and Technology, Government of India, through the Technology Systems Development Programme's (TSDP) at Indian Institute of Science, Bengaluru, under Project No. DST/TSG/AMT/2015/294.

The authors would like to acknowledge National Nanofabrication Centre (NNfC) at Indian Institute of Science, Bangalore, funded by MeitY and DST, Government of India. In addition, Sayak Dutta Gupta and Rajarshi Roy Chaudhuri would also like to thank DST INSPIRE for their fellowship.

DATA AVAILABILITY

The data that support the findings of this study are available within the article.

REFERENCES

[1]N. Ramanan, B. Lee, and V. Misra, Semicond. Sci. Technol. **30**, 125017 (2015).
[2]A. Colon and J. Shi, Solid State Electron. **99**, 25 (2014).
[3]D. D. Nguyen and T.-K. Suzuki, J. Appl. Phys. **127**, 094501 (2020).
[4]S. Dutta Gupta, A. Soni, V. Joshi, J. Kumar, R. Sengupta, H. Khand, B. Shankar, N. Mohan, S. Raghavan, N. Bhat, and M. Shrivastava, IEEE Trans. Electron Devices **66**, 2544 (2019).
[5]S. P. Le, D. D. Nguyen, and T.-K. Suzuki, J. Appl. Phys. **123**, 034504 (2018).
[6]A. Colon, L. Stan, R. Divan, and J. Shi, J. Vac. Sci. Technol. A **35**, 01B132 (2017).
[7]X. Cui, W. Cheng, Q. Hua, R. Liang, W. Hu, and Z. L. Wang, Nano Energy **68**, 104361 (2020).
[8]R. Asahara, M. Nozaki, T. Yamada, J. Ito, S. Nakazawa, M. Ishida, T. Ueda, A. Yoshigoe, T. Hosoi, T. Shimura, and H. Watanabe, Appl. Phys. Express **9**, 101002 (2016).
[9]Y. Li, Y. Guo, K. Zhang, X. Zou, J. Wang, Y. Kong, T. Chen, C. Jiang, G. Fang, C. Liu, and L. Liao, IEEE Trans. Electron Devices **64**, 3139 (2017).
[10]T. Hashizume, K. Nishiguchi, S. Kaneki, J. Kuzmik, and Z. Yatabe, Mater. Sci. Semicond. Process. **78**, 85 (2018).
[11]Z. Yatabe, J. T. Asubar, and T. Hashizume, J. Phys. D: Appl. Phys. **49**, 393001 (2016).

[12]S. Dutta Gupta, V. Joshi, B. Shankar, S. Shikha, S. Raghavan, and M. Shrivastava, in *2019 IEEE International Reliability Physics Symposium (IRPS)* (IEEE, 2019), pp. 1–5.
[13]J. A. del Alamo, A. Guo, and S. Warnock, J. Mater. Res. **32**, 3458 (2017).
[14]D. W. Johnson, R. T. P. Lee, R. J. W. Hill, M. H. Wong, G. Bersuker, E. L. Piner, P. D. Kirsch, and H. R. Harris, IEEE Trans. Electron Devices **60**, 3197 (2013).
[15]P. Lagger, P. Steinschifter, M. Reiner, M. Stadtmüller, G. Denifl, A. Naumann, J. Müller, L. Wilde, J. Sundqvist, D. Pogany, and C. Ostermaier, Appl. Phys. Lett. **105**, 033512 (2014).
[16]Y. Lu, S. Yang, Q. Jiang, Z. Tang, B. Li, and K. J. Chen, Phys. Status Solidi C **10**, 1397 (2013).
[17]R. Stoklas, D. Gregušová, K. Hušeková, J. Marek, and P. Kordoš, Semicond. Sci. Technol. **29**, 045003 (2014).
[18]M. Ťapajna, M. Jurkovič, L. Válik, Š. Haščík, D. Gregušová, F. Brunner, E.-M. Cho, and J. Kuzmík, Appl. Phys. Lett. **102**, 243509 (2013).
[19]Y.-J. Shi, R.-J. Zhang, H. Zheng, D.-H. Li, W. Wei, X. Chen, Y. Sun, Y.-F. Wei, H.-L. Lu, N. Dai *et al.*, Nanoscale Res. Lett. **12**, 243 (2017).
[20]Y. Zhang, M. Sun, S. J. Joglekar, T. Fujishima, and T. Palacios, Appl. Phys. Lett. **103**, 033524 (2013).
[21]Y.-S. Lin and C.-C. Lu, IEEE Trans. Electron Devices **65**, 783 (2018).
[22]A. Rawat, M. Meer, V. kumar Surana, N. Bhardwaj, V. Pendem, N. S. Garigapati, Y. Yadav, S. Ganguly, and D. Saha, IEEE Trans. Electron Devices **65**, 3725 (2018).
[23]B. Chatterjee, C. Dundar, T. E. Beechem, E. Heller, D. Kendig, H. Kim, N. Donmezer, and S. Choi, J. Appl. Phys. **127**, 044502 (2020).
[24]M. Ťapajna and J. Kuzmík, Appl. Phys. Lett. **100**, 113509 (2012).
[25]C. Mizue, Y. Hori, M. Miczek, and T. Hashizume, Jpn. J. Appl. Phys. **50**, 021001 (2011).
[26]Y. Hori, Z. Yatabe, and T. Hashizume, J. Appl. Phys. **114**, 244503 (2013).
[27]E. H. Nicollian and J. R. Brews, *MOS (Metal Oxide Semiconductor) Physics and Technology* (John Wiley & Sons, 1982).
[28]M. Capriotti, P. Lagger, C. Fleury, M. Oposich, O. Bethge, C. Ostermaier, G. Strasser, and D. Pogany, J. Appl. Phys. **117**, 024506 (2015).
[29]J. L. Lyons, A. Janotti, and C. G. Van de Walle, Phys. Rev. B **89**, 035204 (2014).